SUPERCONDUCTING CRITICAL CURRENT

In the application of superconductors, the superconducting critical current density is often the most important parameter in the design and engineering of practical devices. The reason is that the majority of applications for superconducting wires involve building electromagnets, which develop their magnetic field by virtue of the number of ampere-turns in the magnet winding. Examples of electromagnets presently in the marketplace include magnetic resonance imaging (MRI) magnets; high field research magnets; beam-bending, focusing, and detector magnets for high-energy physics research; superconducting energy storage systems; and superconducting motors and generators (1). As the critical current density of the superconducting wire increases, the achievable magnetic field increases, and the amount of superconductor needed for constructing the magnet decreases. Thus, there is a direct driving force to increase the critical current density of superconductors for magnet applications.

As with the critical temperature (T_C) and critical magnetic field (H_{C2}), the critical current density (J_C) marks the limit of the superconducting state. For direct current (dc) densities less than the J_C, the current is carried without resistive losses, and thus no power input. For current densities greater than J_C, a voltage develops along the superconductor, and the zero resistance condition breaks down.

The T_C and H_{C2}, which are both determined by the chemistry and physics of the superconducting system, are relatively unaffected by the processing of the superconductor. The same is not true for the J_C, which can be radically changed within a given superconducting material by varying the fabrication process and therefore the material's microstructure. For example, within the Nb–Ti alloy system, once the composition of the alloy has been chosen, the T_C and H_{C2} are essentially determined. However, by varying the metallurgical treatments of the alloy as it is processed into wire, it is possible to vary the J_C by factors of 1000 or more (2,3). The potential for controlling the critical current density through processing provides materials science researchers with hope for improving the properties of technical superconductors.

In describing the theory of critical current density in superconductors, it will be useful to consider two length scales. The first is the London penetration depth λ, which is the distance over which an externally applied magnetic field penetrates into a superconductor. This is essentially the distance over which we expect to see large changes in the magnitude of the magnetic fields inside the superconductor. The second length scale is the coherence length ξ, which is the distance over which the superconducting order parameter (or alternatively, the density of superelectrons) varies.

In the Ginzburg–Landau theory of superconductivity, the ratio of the penetration depth to the coherence length is called the Ginzburg–Landau parameter κ, where $\kappa = \lambda/\xi$. The Ginzburg–Landau parameter distinguishes between the two broad classes of superconductors; type I, for which $\kappa < 1/\sqrt{2}$, and type II, for which $\kappa > 1/\sqrt{2}$. The high critical current density superconductors are all type II materials, and κ is quite large for many of these materials, on the order of 50 or so.

The remainder of this article describes the measurement of J_C, the basic theory of critical currents in type I and type II superconductors, the flux-line lattice and flux pinning, and thermal effects in determining the J_C. As an overview of a large and complex subject that has occupied many researchers, this article cannot be complete. For a more detailed discussion of general superconductivity, see texts by Rose-Innes (4), Tinkham (5), and especially Orlando (6) for an excellent presentation from an electrical engineering perspective. Detailed surveys of flux pinning and critical current density may be found in the monographs by Campbell and Evetts (7), and Ullmaier (8), which form the basis of much of the discussion following. Although the majority of the references and discussion uses examples from low-temperature superconductivity (LTS), the principles described are also equally applicable to high-temperature superconducting (HTS) materials.

THE RESISTIVE MEASUREMENT OF CRITICAL CURRENT DENSITY

The critical current is usually found by a simple four-point measurement, using the change in the resistance of the sample to determine the transition between superconductivity and normal conductivity (see Fig. 1). The sample, a long coil

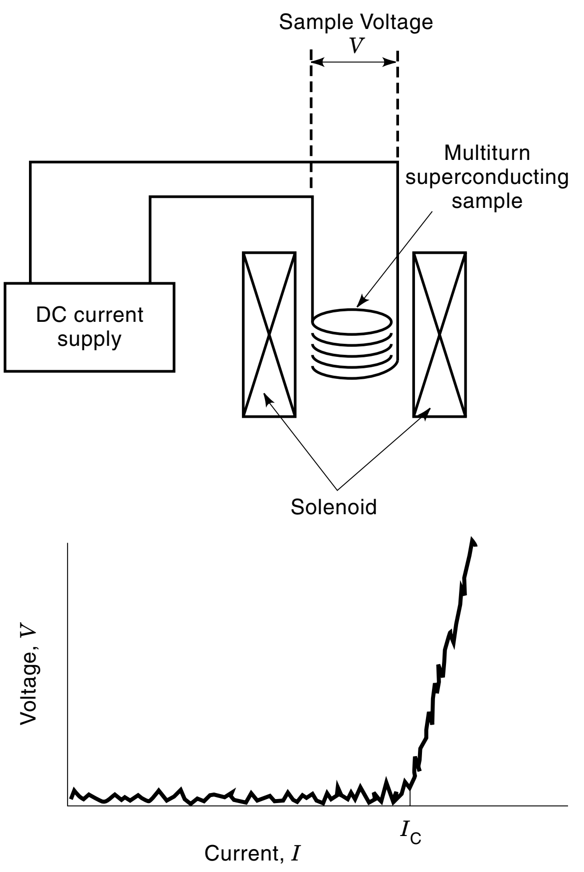

Figure 1. Schematic of the resistive measurement of the critical current density. The superconducting sample in the center of a high magnetic field solenoid produces a voltage when the current exceeds the critical current. The plot shows the $V(I)$ characteristic of the superconducting wire. The critical current I_C is defined at the appearance of a measurable voltage.

of wire, is placed in the bore of a high field electromagnet, and a dc current is passed through it. The voltage along the length of the superconducting wire is measured. A zero voltage indicates superconductivity, whereas a nonzero measurement indicates resistive dissipation and loss of superconductivity. This "resistive" measurement technique may be used to measure critical temperatures by passing a small constant current, varying the sample temperature, and measuring the sample voltage. It can also be used to measure the critical magnetic field H_{C2} of type II superconductors by varying the magnetic field on the sample. Of more concern to the present discussion is measuring the critical current I_C. This is done by holding the sample in a constant magnetic field and increasing the current through the superconductor until a voltage increase is measured (see Fig. 1). In this way the critical current is determined.

As the current is increased through the superconducting wire, the voltage along the wire slowly increases from zero until a rapid increase occurs near the critical current. If the $V(I)$ characteristic is measured over a large enough voltage range, the curve looks like that shown in Fig. 2. Early experiments (9) showed that the $V(I)$ characteristic at high currents becomes linear, and the resistivity depends on the applied magnetic field, roughly following

$$\rho_{\mathrm{ff}} = \left(\frac{H}{H_{C2}}\right)\rho_{\mathrm{n}} \quad (1)$$

where ρ_{ff} and ρ_{n} are the high current resistivity (flux flow resistivity) and normal state resistivity of the superconductor, respectively. This linear region at high currents is called the "flux-flow" regime for reasons that are described following.

Eventually, the increasing power dissipation due to the flux flow resistivity causes the temperature of the superconductor to rise above T_C and there is a phase transition to the normal state (Fig. 3). An important point to note is that within the flux flow regime the sample is still superconducting, though it is no longer in the zero dissipation (or zero resistance) condition.

Empirically it has been found that the shape of the $V(I)$ curve at low voltages (well below the linear flux-flow regime)

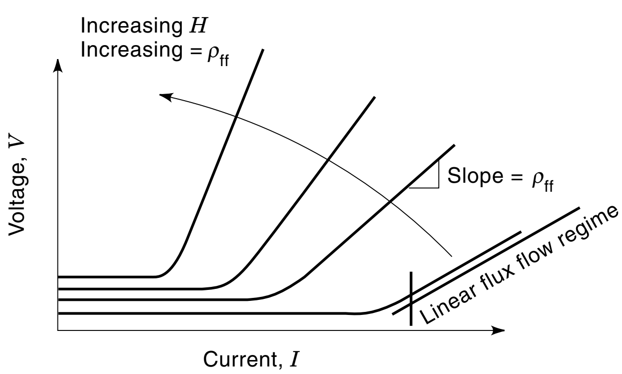

Figure 2. Schematic of the voltage versus current measurement of the critical current of a superconducting wire as a function of the applied magnetic field. The zero voltage points have been offset for clarity. As the field increases, the critical current decreases, and the high current slope ρ_{ff} increases.

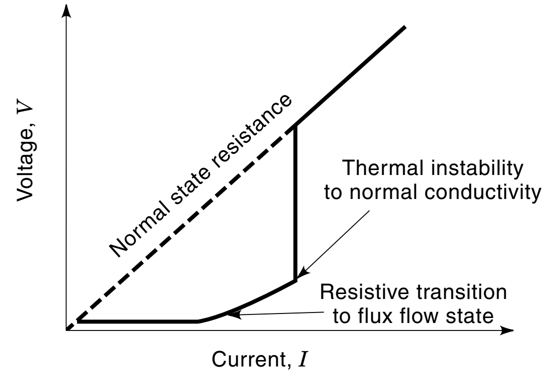

Figure 3. Schematic of the full $V(I)$ characteristic of a superconducting wire. At low currents the superconductor exhibits zero resistance and zero voltage. At the critical current there is a transition into the flux-flow regime, and the voltage increases. At larger currents, ohmic heating causes the temperature to rise above the critical temperature, and the sample thermally runs away to the normal state resistance behavior.

can be described by a power law

$$V(I) = K\left(\frac{I}{I_C}\right)^n \quad (2)$$

so that a plot of log$V$ versus log$I$ from the I_C measurement yields a straight line whose slope is sample-dependent and also depends on the applied magnetic field (10). Recent measurements on high temperature superconducting (HTS) materials also show this power law behavior. Typically HTS materials are measured over a much larger range of current and voltage than is usual in the LTS materials (11,12).

Over the years of development of LTS wires, it has been empirically determined that larger slopes of the log V versus log$I$ plot were correlated with higher current density or higher "quality" superconducting wires. This slope has come to be known as the "n-value" of a wire and is commonly reported by LTS wire manufacturers. Values of n between 40 and 100 are generally considered to indicate good quality wires. From Eq. (2) one can see that, as the n-value for a wire increases, the transition from the zero resistance state to the flux flow state becomes steeper and narrower.

Because of the gradual transition from zero voltage to the linear flux-flow regime, the critical current is usually determined by using a standard measurement criterion. For many years magnet designers preferred a constant resistivity criterion, for example, $\rho = 10^{-14}$ Ω-m. A line is drawn on the $V(I)$ data plot with a resistive slope corresponding to 10^{-14} Ω-m, based on the dimensions of the sample. The intersection of this line with the $V(I)$ measurement is the critical current I_C. Because the $V(I)$ characteristic is curved, the measured value of the I_C depends on the criterion used, so this information must be provided along with the measurement value. Historically, the 10^{-14} Ω-m criterion has been used by magnet designers because it was found that early superconducting magnets thermally ran away to the normal state (quench) at a magnet resistivity of about 10^{-14} Ω-m. A second commonly used criterion is the constant electric field criterion, in which the I_C is given by the current at which the $V(I)$ measurement exceeds a constant electric field value, for instance, 10 μV/m.

It is important here to draw a distinction between the critical current I_C, which has units of amperes, and the critical current density J_C, which has units of amperes per unit cross-sectional area. The fundamental property of the superconducting state is the J_C, which is the maximum current per unit cross-sectional area of superconductor that is carried without resistive losses. The J_C is determined by measuring the critical current I_C of the specimen and dividing by the cross-sectional area of the superconductor: $J_C = I_C/A$.

An additional definition of importance is the engineering J_C which is defined as the maximum transport current per unit cross section of superconducting wire. Most technological superconductors are fabricated as a composite of superconducting and normal metal for thermal and mechanical stability (1,13). For the magnet designer, the engineering J_C (sometimes abbreviated as J_E) determines the available current in the magnet windings. The distinction between J_C and J_E is especially important when magnet designers are working with superconducting composites in which the superconducting area is a small fraction of the total wire cross section, as in tape composites and many early HTS wires.

It is also worthwhile at this point to describe the difference between transport currents and shielding currents. Superconductors placed in a magnetic field exclude some or all of the magnetic flux from the bulk of the superconductor (known as the Meissner–Ochsenfeld effect). For this exclusion to occur, shielding currents flow on the surface of the superconductor such that the magnetic field produced by the shielding currents opposes the applied field and cancels it out. In general, the shielding currents flow in loops that are closed entirely within the superconductor. In contrast, transport currents are those currents applied from outside the superconductor using external current sources. The transport currents are the currents used to produce magnetic fields in the superconducting magnets and to make the resistive measurements of the critical parameters of superconductivity.

With this basic understanding of how the J_C is typically measured we can begin to discuss the physical mechanisms limiting J_C in practical materials.

ULTIMATE LIMITS TO J_C: THE DEPAIRING CRITICAL CURRENT DENSITY

In the Bardeen–Cooper–Schrieffer theory of superconductivity, the charge carriers are pairs of electrons bound together by a positive electron–phonon interactive force. The bonding energy of the superelectron pair at zero kelvin is denoted as the energy gap $\Delta(0)$. The critical temperature can be determined from the energy gap as the temperature at which the thermal excitation energy kT is equal to the energy gap bonding the superelectron pair together. More rigorously this relationship is

$$2\Delta(0) = 3.5\,kT_C \tag{3}$$

The superconductivity stops because the thermal energy is sufficient to "depair" or "decouple" the superelectrons.

Similarly, the thermodynamic critical magnetic field H_C at zero kelvin can be determined from the energy gap by using the magnetic free energy difference between the normal and superconducting states:

$$\frac{1}{2}\mu_0 H_c^2 = \frac{1}{2}N(\epsilon_F)[\Delta(0)]^2 \tag{4}$$

where $N(\epsilon_F)$ is the density of states at the Fermi energy and μ_o is the permittivity of free space. Thus, the critical magnetic field is that magnetic field for which the magnetic energy is large enough to break apart the electron pair.

In a similar approach to the arguments used to estimate T_C and H_C, one would expect that there is an ultimate critical current density limited by the kinetic energy of the superelectron pairs in a transport current. When the kinetic energy of the electrons exceeds the energy gap, the pairs break apart and become normal (resistive) charge carriers. The kinetic energy of the superelectrons can be written as

$$\mathrm{KE} = \frac{(m^* v_F^2)}{2} = \frac{p_F^2}{2m^*} \approx 2\Delta(0) \tag{5}$$

where m^* is the effective mass of the charge carriers (in this case $m^* = 2m_e$, two times the mass of an electron), and v_F and p_F are the Fermi velocity and momentum, respectively.

The current density produced by these charge carriers is given by

$$J = qn_s v = 2en_s v_F \tag{6}$$

where q is the charge of the current carrier (= $2e$ for electron pairs) and n_S is the density of superelectron charge carriers.

The depairing critical current density can be found by combining Eqs. (5) and (6):

$$J_D \approx \frac{10\,en_s\Delta(0)}{p_F} \tag{7}$$

Orlando (6) derives an equivalent form of Eq. (7) from Ginzburg–Landau theory as

$$J_D = \frac{\phi_0}{3\sqrt{3}\pi\mu_0\lambda^2\xi} \tag{8}$$

where λ and ξ are the penetration depth and coherence length, respectively, and ϕ_o is the magnetic flux quantum. Using either Eqs. (7) or (8) we can calculate the depairing critical current density shown in Table 1 at zero kelvin and zero magnetic field for several superconducting systems.

As can be seen from Table 1, the depairing critical current densities are quite large, especially when compared with the typical current density in standard copper household wiring of about 10^7 A/m^2. The superconducting materials shown here have theoretical critical current densities at least 10^4 times

Table 1. Theoretical Depairing Critical Current Density[a]

Superconductor	λ, nm	ξ, nm	J_D, A/m^2
NbTi	300	4	2×10^{11}
Nb_3Sn	65	3	8×10^{12}
YBa_2Cu_3O (*ab* plane)	30	3	4×10^{13}
YBa_2Cu_3O (*c* plane)	200	0.4	6×10^{12}

[a] Calculated using Eq. (8) for several important superconductors.

larger than copper. It is because of these large values of critical current density with no resistive losses (and therefore no power dissipation) that superconductors are so important in large electromagnet applications (1).

It should be remembered that the values of J_D listed in Table 1 are calculated for zero kelvin and zero magnetic field, and in practice these conditions do not hold. In fact, these values of current density have never been reached because of other practical limitations. One of these limitations is the self-field produced by a wire carrying a transport current. As the transport current through the wire is increased, the self-field at the surface of the superconductor increases. At some point, the magnetic field due to the transport current becomes equal to the critical magnetic field of the wire, and the superconductivity breaks down. This model of the practical limit to J_C is know as Silsbee's hypothesis (14), and is usually applied to find the critical current limit of type I superconductors.

Of greater technological importance than the Silsbee limit in type I materials is the limitation of the J_C in type II superconductors because type II superconductors display superconductivity up to larger magnetic field values than type I superconductors. To understand the factors limiting the J_C in type II materials, it is necessary to review the magnetic properties of these superconductors and introduce the concept of the flux-line lattice.

THE MAGNETIC FLUX LINE LATTICE

The principal difference between type I and type II superconducting materials lies in their response to an applied magnetic field. Type I superconductors exclude an applied magnetic field from the body of the superconductor up to the thermodynamic critical field H_C. To exclude this magnetic flux, a shielding current is established on the surface of the superconductor that flows in a direction so as to produce a flux density equal and opposite to the applied field. This surface current flows in a surface layer whose thickness is equal to the magnetic penetration depth λ. The magnitude of the surface current can be found by using Ampere's law which states that the spatial variation in the magnetic field is proportional to the current density flowing:

$$\nabla \times \boldsymbol{H} = \boldsymbol{J} \tag{9}$$

where both $\boldsymbol{H}$ and $\boldsymbol{J}$ are vector quantities. For the one-dimensional case of a semi-infinite slab of type I superconductor in the y–z plane, and an applied field H, parallel to the slab in the z-direction, Ampere's law becomes

$$dH_z/dx = J_y \tag{10}$$

Because the magnetic field decays over a length λ into the superconductor, we know that the applied field and the shielding current density are related approximately as

$$\frac{H_A}{\lambda} = J_y \tag{11}$$

As the magnitude of the applied field increases, the magnitude of the current density increases to shield the superconductor from the field. The maximum current density is obtained when the applied field at the surface of the type I superconductor is equal to H_C, in which case $J_{MAX} = H_C/\lambda$. This shielding current density is the same as the depairing current density described by Eqs. (7) and (8).

The shielding currents in the type I superconductor effectively provide a diamagnetic magnetization, $M = -H_A$, as shown in Fig. 4(a), called the Meissner–Ochsenfeld effect.

For type II superconductors, the magnetic response is somewhat different. Up to a lower critical field H_{C1}, the magnetic response of type II superconductors is the same as that of type I and shows a full flux expulsion, with $M = -H_A$ (see Fig. 4b). In this region, the superconductor is said to be in the Meissner state. For magnetic fields higher than H_{C1}, the magnetic free energy balance of the superconductor makes it energetically favorable for the magnetic field to enter the bulk of the superconductor. As the magnetic flux enters the bulk superconductor, it breaks into quantized units of flux ϕ_0, variously called the flux quantum, fluxon, fluxoid, flux vortex, or flux line. The flux quantum has a magnitude of ϕ_0, $= 2.0679 \times 10^{-15}$ T-m^2.

The individual flux quanta, or flux lines, orient themselves parallel to the applied field and effectively reduce the magnetization of the type II superconductor below that of the perfect diamagnetism of the Meissner state. This state of lower magnetization is called the mixed state. As the applied field increases, the number of flux lines per unit area increases in the superconductor and M approaches zero. Eventually the

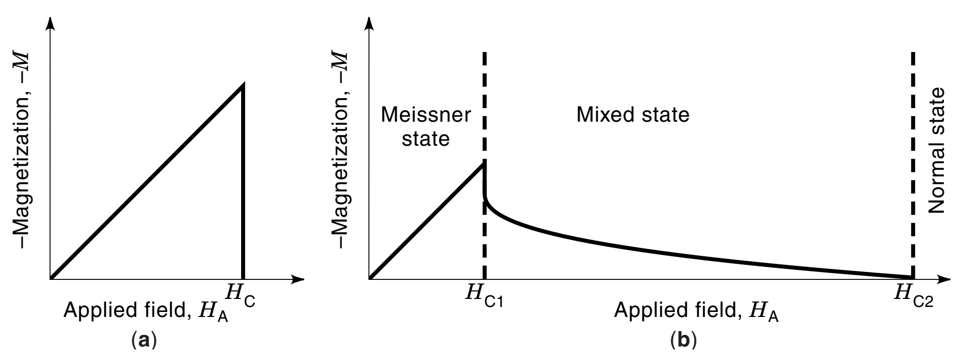

Figure 4. The magnetic behavior of type I and type II superconductors. Type I superconductors exclude the applied field from the bulk of the superconductor by producing a supercurrent on the surface to cancel the applied field, yielding the magnetization versus field plot shown in (a). Type II superconductors exclude the applied field up to a lower critical field H_{C1} and then allow the field to enter the bulk as flux quanta ϕ_o, until the upper critical field H_{C2} is reached (b). At this point the superconductivity is destroyed by the applied field.

flux lines touch one another, and the field inside the superconductor becomes equal to the applied magnetic field, driving the magnetization to zero at the upper critical magnetic field H_{C2}. The superconducting material remains superconducting up to large values of the applied magnetic field (H_{C2}), and this is one of the main reasons that the type II materials are used for electromagnet applications.

The interaction of the individual flux lines with one another is similar to that of two parallel bar magnets. Because the orientation of the field in the flux lines is the same, they repel one another strongly. This causes the flux lines to distribute themselves in a periodic lattice to minimize the interflux line interactions (Fig. 5). This periodic structure, called the flux line lattice (FLL), was theoretically predicted by Abrikosov (15) using extensions of the Ginzburg–Landau theory of superconductivity. Abrikosov found that the lowest free energy configuration for the FLL is a triangular or hexagonal "crystal." The FLL has been experimentally verified in several ways, including magnetic particle decoration techniques (16) and diffraction from the flux line crystal by using the magnetic moment of neutrons (17). The magnetic decoration technique, in particular, provides a striking visualization of the periodicity of the flux line lattice, as shown in Fig. 6.

We can model an isolated flux line as a cylindrical core of normal-phase material in which the superconductivity has been destroyed by the magnetic field and which is surrounded by a circulating supercurrent. The magnetic flux resides within the core and decays into the bulk of the superconductor over a distance of the magnetic penetration depth λ (Fig. 7). Within this range, the local magnetic field strength H is changing, and therefore, by using Ampere's law [Eq. (9)], there is a current flowing in the superconductor. This current is analogous to the shielding current that flows on the superconductor surface to exclude the magnetic field. In this case it is a circulating current that flows around the flux-line core and has an orientation and magnitude needed to produce the ϕ_0 of magnetic flux in the core (Fig. 7). This circulating current is the origin of the name "flux vortex."

The cylindrical core has a diameter twice the coherence length (2ξ). The coherence length is the distance over which the superconducting order parameter $|\psi|^2$ (or the density of superconducting electron pairs n_S) changes from its maximum value at the core radius to zero in the center of the core (Fig. 7). The field strength in the core can be estimated as the magnetic flux divided by the cross sectional area of the flux line:

$$H_{\mathrm{CORE}} = \frac{\phi_0}{\mu_0 \pi \xi^2} = H_{C2} \tag{12}$$

As we introduce more flux lines into the interior of the superconductor, the circulating supercurrents of the neighboring flux lines begin to interact and repel one another, leading to the periodic structure of the flux-line lattice. The flux density

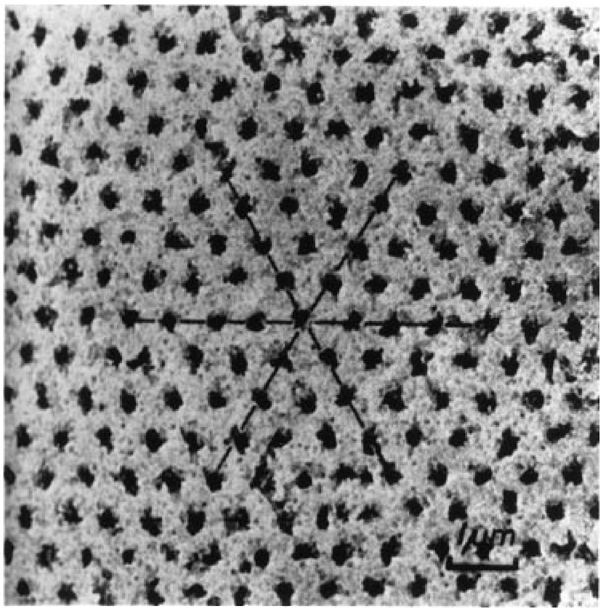

Figure 6. The magnetic flux line lattice imaged using a magnetic particle decoration technique. The small scale magnetic particles are attracted to the regions of large flux gradient at the flux line cores and then can be imaged by transmission electron microscopy. The periodic triangular flux line lattice can be clearly distinguished. Reprinted with permission from H. Trauble and U. Essmann, *J. Appl. Phys.,* **39**(9): 4052–4056, 1968. Copyright 1968, American Institute of Physics.

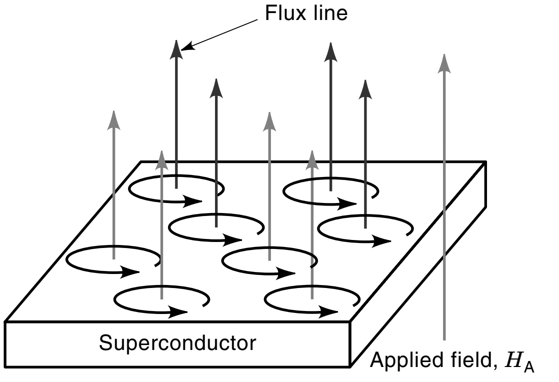

Figure 5. Schematic of the magnetic flux line lattice in a type II superconductor for applied fields between $H_{C1} < H_A < H_{C2}$. The flux lines arrange themselves in a triangular or hexagonal lattice due to the inter-flux-line magnetic repulsive forces.

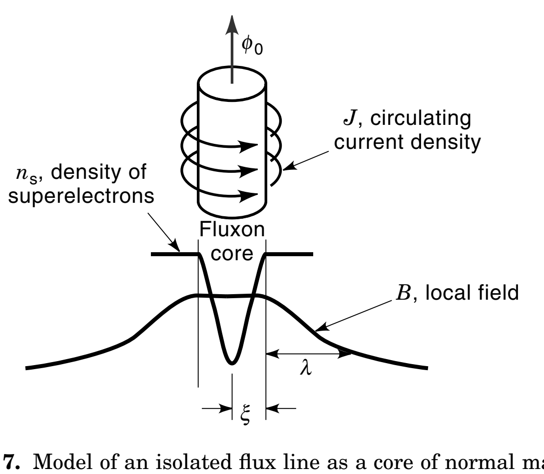

Figure 7. Model of an isolated flux line as a core of normal material containing the magnetic flux quantum ϕ_0. The magnetic field falls off over a distance of λ, the penetration depth. The core has a radius of ξ, the superconducting coherence length, and the density of superelectrons falls to zero at the center of the flux line core.

at any point in the superconductor is found from the number density of flux lines as $B = n_\phi \phi_o / A$, where n_ϕ is the number of flux quanta in the cross-sectional area A. In a homogeneous type II superconductor in the mixed state (i.e., in an applied field between H_{C1} and H_{C2}), the magnetic flux breaks up into flux lines, each containing one quantum (ϕ_o), of magnetic flux that are periodically arranged in this two-dimensional "crystal" lattice.

If a transport current is applied to such a superconducting wire, where the current flow is along the axis of the wire and the applied magnetic field is perpendicular to the axis (as shown in Fig. 8), there is an interactive force between the flux lines and the transport current. Lorentz's law for the force on a charged particle moving through a magnetic field is given by

$$\boldsymbol{F}_{\mathrm{L}} = \boldsymbol{J} \times \boldsymbol{B} \tag{13}$$

where $\boldsymbol{F}_{\mathrm{L}}$ is the Lorentz force density acting between the current of $\boldsymbol{J}$ and the flux density $\boldsymbol{B}$. The $\boldsymbol{F}_{\mathrm{L}}$ has units of Newtons per cubic meter and acts in a direction perpendicular to both the flux density $\boldsymbol{B}$ and the transport current density $\boldsymbol{J}$ (Fig. 8).

The result of the Lorentz force acting on the FLL is to push the flux lines across the superconductor. The movement of the flux lines corresponds to a change in the flux density within the superconducting circuit with time (Fig. 1), and from Maxwell's equations for such a case (6),

$$\frac{d\boldsymbol{B}}{dt} = -\nabla \times \boldsymbol{E} \tag{14}$$

In other words, the moving magnetic flux lines produce an electric field gradient (or voltage) in the direction of the transport current flow. As the FLL moves, a voltage is generated that must be supplied by the external power supply. The consequence of this flux motion is that the superconductor no longer supports a transport current with zero dissipation, and therefore the zero resistance state no longer exists.

It is important here to draw a distinction between the loss of the superconducting state and the loss of the zero resistance condition. As long as the superconductor remains in fields less than the upper critical field H_{C2} at temperatures lower than T_C and carries transport currents less than J_D, it is in the superconducting state. The nonzero resistance occurs only because the FLL is moving under the Lorentz force produced by the transport current and changing the magnetic flux linked by the superconductor. This is the "flux-flow" regime described earlier. If we could prevent the FLL from moving because of the Lorentz force, the zero resistance condition would persist to higher transport currents, effectively increasing the critical current density.

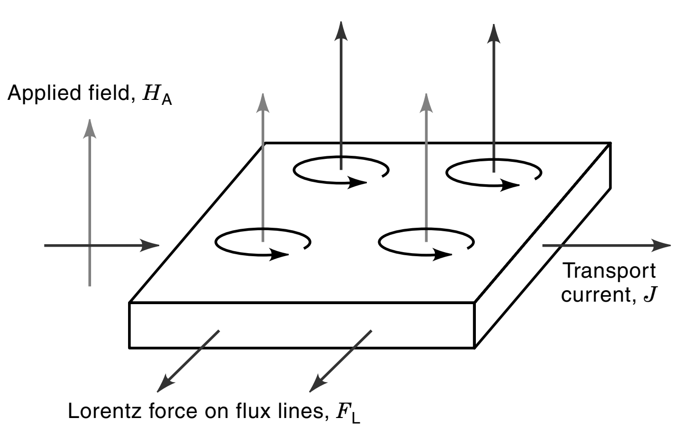

Figure 8. The orientation of the magnetic field, transport current, and Lorentz force acting on the flux line lattice. The Lorentz force between the flux lines and the transport current causes the flux lines to move across the superconductor.

The bulk pinning force density F_P (N/m^3), is defined for samples carrying a transport current in a transverse field as the critical Lorentz force:

$$\boldsymbol{F}_{\mathrm{P}} = |\boldsymbol{F}_{\mathrm{LC}}| = \boldsymbol{J}_{\mathrm{C}} \times \boldsymbol{B} \tag{15}$$

where $\boldsymbol{J}_{\mathrm{C}}$ is the current density at which voltage losses occur in the superconductor.

In essence, holding the FLL against the Lorentz force adds a transition line for the change from flux pinning to flux flow to the phase diagram of the type II superconductor in Fig. 9. The solid lines represent thermodynamic phase transitions between the superconducting (Meissner and mixed) states and the normal state, and the dashed line shows the transition from the flux-pinning (zero resistance) condition to the dissipative flux-flow condition.

Ideally, one would like to move the dashed line up in current density as close to the phase transition line (determined by J_D) as possible. This is the goal of the flux pinning discussed in the next section.

FLUX PINNING

To increase the current that a superconductor may carry without power dissipation, it is necessary to restrain the FLL against the Lorentz force by "pinning" it in place. There are several mechanisms by which the FLL may be pinned, and generally these rely on developing microstructural features that interact with the individual flux lines. Examples of microstructural features that provide pinning resistance to the Lorentz force include normal conducting precipitates, inclusions, voids, and grain boundaries.

The basic theory of flux pinning in type II superconductors is conveniently broken into three sections. These are basic interactive forces, summation theory, and scaling laws (7,8).

Basic Interactive Forces

The basic interactive forces are the forces between single, isolated flux lines and individual pinning centers. The usual model for the basic interactive force is that the pinning center must provide a spatial variation of the thermodynamic free energy of the flux line. This can be visualized as either an energy well (Fig. 10) or an energy hill. In the case shown in the upper part of Fig. 10 the flux line has a lower free energy when it sits in the energy well of the pinning center than it does in the bulk superconductor, and thus there is a pinning force holding the flux line in the well. The pinning force is related to the free energy by the first derivative with respect to position, so that the pinning force curve looks like that shown in the lower part of Fig. 10. The deeper the potential

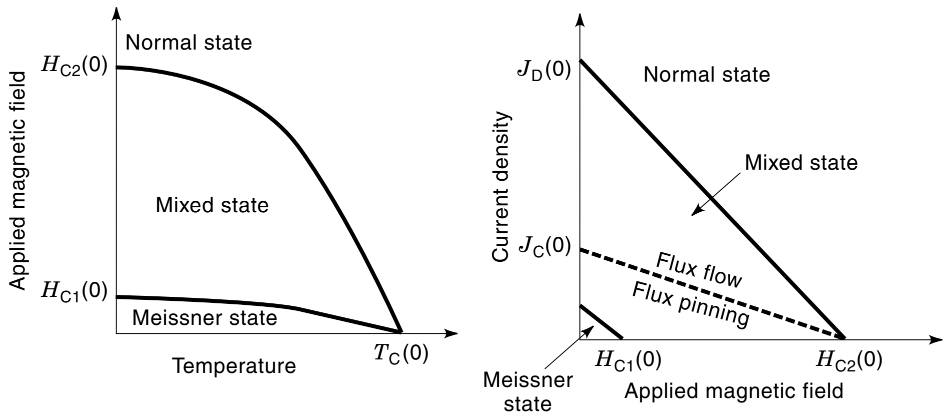

Figure 9. The H–T and J–H phase diagrams for type II superconductors. At low applied fields the superconductor is in the Meissner state. At higher fields the superconductor enters the mixed state with the creation of the flux line lattice (FLL). As the transport current is increased from zero, the Lorentz force on the FLL eventually causes it to move, causing flux-flow dissipation and a resistive voltage, shown as the dotted line. The superconducting state does not end until the current density exceeds the depinning current density or the temperature rises above T_C. As flux pinning increases, the transition to flux flow occurs closer to the depairing critical current density limit.

well, the steeper the energy profile, and the larger the pinning force.

If a Lorentz force is applied to a flux line trapped in this potential well, the flux line moves in the direction of the Lorentz force until it is balanced by the oppositely directed pinning force. Thus the flux line is held in place, there is no flux movement, and Eq. (14) shows that there is no dissipation. The transport current is carried without power dissipation, and the zero resistance condition is in effect. Superconducting materials that pin magnetic flux are sometimes called "hard" superconductors analogous to engineering alloys that have been mechanically hardened by treatments to pin the movement of dislocations.

One type of basic interactive force between a single flux line and a single pinning center is called the core interaction. To nucleate a flux line within the superconductor, the system

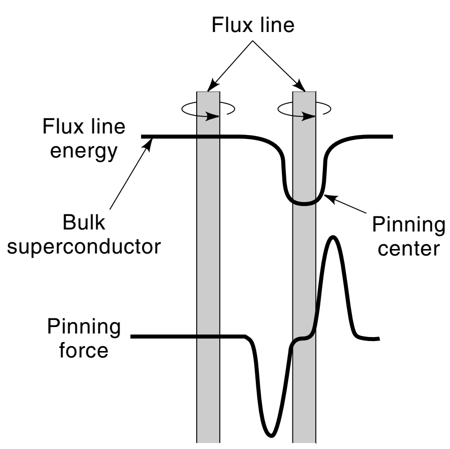

Figure 10. The variation in the free energy of the flux line in the vicinity of a pinning center. The energy well produces a net force on the flux line centering it in the pinning center and constraining it against the Lorentz force of the transport current.

must provide enough energy to convert the core of the flux line to the normal state. This energy (per unit length of flux line), called the condensation energy, is given by the volumetric free energy due to the magnetic field within the flux line and the cross-sectional area of the fluxon core as

$$E_{\mathrm{COND}} = \left(\frac{\mu_0 H_C^2}{2}\right)\pi\xi^2 \tag{16}$$

where H_C is the thermodynamic critical field and ξ is the superconducting coherence length.

Imagine that the superconductor contains a cylindrical void of diameter 2ξ and its axis is oriented parallel to the flux-line axis. If the flux line were centered on this void, the condensation energy needed to produce the normal core of the flux line would be saved, and the flux line would see a lower free energy at the location of the void than it would in the bulk, similar to Fig. 10. The result of this free energy change is that the flux line requires an increase in its energy per unit length equal to the condensation energy, Eq. (16), to move away from the void. Thus the void acts as a pinning center holding the flux line in place.

As the current density is increased, the Lorentz force on the pinned flux line increases until it exceeds the maximum gradient of the free energy versus position curve (Fig. 10). At this point the flux line is free of the pinning center and moves under the Lorentz force, creating a dissipative loss due to Eq. (14).

There are many different interactions between the flux line and microstructural defects that lead to basic interactive forces and pinning. The core interaction may be applied to voids and also to normal conducting precipitates (as in the Nb–Ti system) or weakly superconducting inclusions, for which there is a spatial dependence of the superconducting condensation energy. A different interaction that is thought to be important in flux pinning in single-phase superconduc-

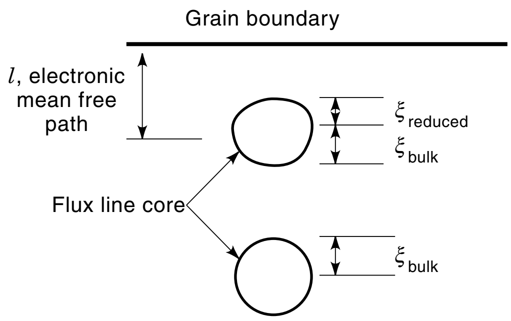

Figure 11. The superconducting coherence length is reduced within an electron mean free path of a scattering defect, such as a grain boundary. This causes the flux line core to distort so that the volume of the flux line changes as it approaches the grain boundary. The variation of the flux-line energy with distance from the grain boundary causes a pinning interaction between the flux line and the grain boundary.

tors, such as Nb_3Sn, is the grain boundary interaction, first proposed by Zerweck (18).

In the grain boundary interactive model, the grain boundaries are viewed as strong scattering centers for the normal electrons in the metal, thereby reducing the mean free path of the electrons near the grain boundary. When the electron mean free path l is less than the coherence length, the coherence length depends on the mean free path as

$$\xi_{\text{dirty}} = 0.85(\xi_0 l)^{1/2} \tag{17}$$

This is often referred to as the "dirty limit" since the mean free path of the electrons is much shorter than that of a "clean" high-purity metal (5).

From Eq. (17), the coherence length is reduced within an electron mean free path of the grain boundary. The effect of the change in the coherence length is that as the flux line core moves closer to the grain boundary, it becomes deformed (Fig. 11) and changes its volume so that the total energy (condensation energy times the core volume) changes with distance from the grain boundary. The free energy difference with position leads to a pinning force, as with the core interactive model.

A more general approach to basic interactive forces derives from the Ginzburg–Landau theory of superconductivity, which can be written to show that the variation in the free energy of a flux line depends on spatial variations of the critical field and the Ginzburg–Landau parameter κ. One version of this derivation (7) is to write the variation in the free energy of the flux line due to pinning defects as

$$\delta E = \int \mu_0 H_C^2 \left[-\left(\frac{\delta H_{C2}}{H_{C2}}\right) |\psi|^2 + \frac{1}{2}\left(\frac{\delta \kappa^2}{\kappa^2}\right) |\psi|^4 \right] dV \tag{18}$$

where ψ is the unperturbed order parameter of the superconductor.

From this perspective, any spatial variation in either critical field (dH_{C2}/H_{C2}) or κ ($d\kappa/\kappa$) produces a change in the free energy of the flux line that leads to a basic interactive force for pinning. Examples of pinning defects of this sort include normal and weakly superconducting inclusions and precipitates, dislocation clusters (subgrain boundaries), and chemical inhomogeneities, which produce pinning interactions through changes in the electron mean free path and therefore affect κ through the coherence length.

A class of basic interactive forces that can be modeled using "image" vortices to calculate the pinning forces are grouped together as magnetic interactions. In these cases the interaction between the circulating supercurrents and microstructural defects leads to pinning forces, rather than interactions involving the normal core. An example is the pinning force between a flux vortex and an electrically insulating plane. The interactive force is calculated by introducing an identical "image vortex" on the opposite side of the insulating plane. The overlapping supercurrents of the real flux line and the image vortex repel one another and produce a force between the flux line and the insulating plane.

A recent addition to the theory of basic interactive forces is that of the Josephson vortex (19,20). The Josephson vortex model accounts for the large pinning forces found in optimized Nb–Ti alloys for which the pinning centers are thin sheet-like ribbons of normal conducting α-Ti. These ribbons are much thinner than the flux line core, so that the core interaction does not accurately describe the pinning interaction. At the same time, the ribbons are not insulators, so that the magnetic interaction also does not apply. The model estimates the basic interactive force by considering what happens to the circulating supercurrent around the flux line, as it approaches a normal conducting planar pinning center. Given that the supercurrent cannot readily penetrate the (normal) pinning plane, the supercurrent spreads out along the planar defect, slowly tunneling through the pinning plane as a superconducting Josephson tunneling current to complete the current loop on the other side of the pinning plane (Fig. 12). The effect is that the flux line becomes distributed over a broad area of the pinning plane and produces a pinning force due to the Josephson current interactions.

In summary, basic interactive forces can arise from many different physical mechanisms, of which only a few have been described here. By providing a spatial variation in the free energy of the individual flux lines, the pinning centers produce a pinning force that holds the flux lines stationary against the Lorentz force, thus increasing the critical current density of the superconductor.

Summation Theory

The second key part in the discussion of flux pinning is summation theory. Given a model for the basic interactive forces between individual pinning centers and individual flux lines, now we must consider the effect of large numbers of flux lines

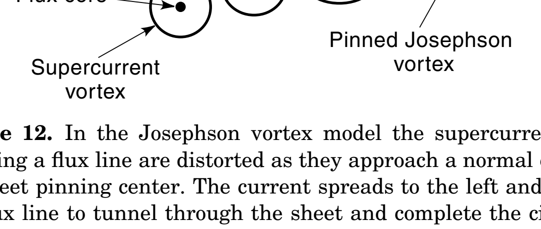

Figure 12. In the Josephson vortex model the supercurrents surrounding a flux line are distorted as they approach a normal conducting sheet pinning center. The current spreads to the left and right of the flux line to tunnel through the sheet and complete the circuit on the opposite side. When the flux line rests on the sheet, it spreads out along the length of the pinning center, losing the normal core and distributing the flux quantum over a large area.

interacting with large numbers of pinning centers. The principle complication of summation is that the flux lines interact repulsively with one another and, in the absence of a pinning force, order themselves in the flux line lattice. Thus, the flux line lattice acts as a two-dimensional, elastic, crystalline solid.

If the inter-flux-line forces are weak compared to the basic interactive forces with the pinning centers, then the individual flux lines move out of the periodic FLL and arrange themselves so that as many flux lines as possible are located on the pinning centers. If the number density of flux lines is less than or equal to the number of pinning centers (for instance, at small applied fields), then each flux line is individually pinned, and the bulk pinning force is large. This is called direct summation, and the bulk pinning force density is just the number density of pinning centers times the basic interactive force.

At the other extreme in which the interaction between the flux lines in the flux line lattice is infinitely strong, the FLL is completely rigid, and there can be no bulk pinning force due to a collection of randomly distributed pinning centers because, for any position of the FLL relative to the random array of pinning centers, there will be as many basic interactive forces pulling the FLL to the left as to the right, and the bulk pinning force density averages to zero. Even though the basic interactive forces are very large, if the FLL acts as a rigid solid because of interfluxon forces, there will be no bulk pinning force, and the FLL will move under the Lorentz force due to the transport current, yielding a low J_C.

The correct description of pinning certainly lies somewhere between these two extremes of direct summation and the rigid FLL lattice. There are several models proposed to account for the summation of the basic interactive forces, and all of them depend strongly on the elastic properties of the FLL as determined by the inter-flux-line forces. In essence, the FLL is a crystalline solid that is placed under an external load by the competition of the transport-current-induced Lorentz forces and the restraint of the pinning forces. As the Lorentz force loading increases, the FLL elastically distorts until either the pinning forces are exceeded, at which point the entire FLL breaks free and moves in unison through the superconductor, or the load overcomes the inter-flux-line forces, and the periodic FLL breaks apart.

This is analogous to mechanically loading a tensile specimen above its elastic limit and into the plastic deformation region. As the mechanical test specimen is plastically distorted, crystalline defects in the specimen are created (dislocations), and the mechanical properties depend strongly on the presence of these crystal defects. In the superconductor with pinning centers, the increasing Lorentz force begins to introduce crystal defects which fragment the FLL into a polycrystalline FLL. The crystalline nature of the FLL has been experimentally observed, as has the polycrystalline and defective FLL, by using both magnetic particle decoration techniques and neutron scattering (21,22). It is also the case that the presence of FLL crystal defects strongly affect its mechanical properties and response to Lorentz force loading (7).

There have been several calculations of the elastic behavior of the FLL. An example is shown in Fig. 13 (8,23) for a NbTa alloy superconductor. C_{11} is the elastic modulus in the plane normal to the flux line axes. This is a measure of the stiffness of the FLL while pushing the flux lines closer together. C_{44} is the elastic tilt modulus which describes the bending of flux lines along their axis. C_{66} is the shear modulus, which describes the resistance of the FLL to the shear of flux lines past one another. An excellent discussion of the effect of the FLL elastic constants on the deformation of the flux line lattice may be found in Ref. 8.

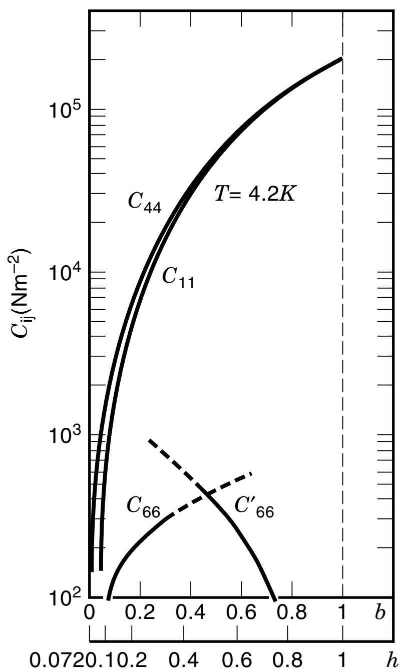

Figure 13. Labusch calculation of the elastic constants of the flux line lattice in Nb–Ta. Notice that the C_{11} and C_{44} elastic constants increase with magnetic field, whereas the shear modulus C_{66} decreases with field at high fields. The b and h are the reduced fields B/B_{C2} and H/H_{C2}, respectively. Reprinted with permission from Ref. 8.

When the number density of flux lines is larger than the number density of pinning centers (as is often the case), there are two primary models of the summation behavior of the FLL. These are the flux line lattice shear model and the collective-pinning model.

In the FLL shear model, individual flux lines are strongly pinned on individual pinning centers, and the excess flux lines not directly pinned are held in place against the Lorentz force due to the interfluxon forces. At large enough transport currents, the Lorentz force becomes larger than the elastic shear modulus (C_{66}) can support, and the FLL shears, allowing unpinned flux lines to flow between those strongly pinned by the pinning centers. Therefore the critical current is determined, not by the strength of the pinning forces, but by the shear stiffness of the FLL, given by C_{66}.

In the Brandt model of the flux line elastic constants, the compressive modulus C_{11} and the tilt modulus C_{44} both depend on the magnetic field roughly as

$$C_{11} \approx C_{44} \approx \frac{H^2}{4\pi} \tag{19}$$

whereas the shear modulus near H_{C2} is approximated by

$$C_{66} \approx K\left(1 - \frac{H}{H_{C2}}\right)^2 \tag{20}$$

where K is a proportionality constant. At high magnetic fields, the FLL is very stiff in bending and compression, but becomes softer and softer in shear as the field approaches H_{C2}. Therefore from this summation model one would expect that the high field critical current density would be determined by the FLL shear and would be somewhat independent of the basic pinning interaction. A detailed model of the FLL shear mechanism developed by Kramer (24,25) predicts a different high field behavior of the bulk pinning force density compared to the predictions of the simple direct summation model. Both kinds of behavior have been experimentally observed.

An alternative model for summation that applies in the limit of a larger number density of flux lines than pinning centers is the collective-pinning model (26,27). In collective-pinning theory, the FLL is thought to consist of a polycrystalline collection of "grains" in which the periodic order of the flux line lattice is reasonably well maintained by inter-flux-line forces, but the neighboring grains are uncorrelated with one another. Within a flux lattice grain, the flux lines are strongly pinned to one or more pinning centers, and the correlated group is held in place by the combined action of the basic pinning forces and the inter-flux-line forces.

In the collective-pinning model, the size of the correlated FLL grains is determined by the number density of pinning centers and the relative strength of the pinning force and the inter-flux-line forces. In one limit, where the inter-flux-line forces are large compared to the pinning forces, the flux lattice is elastically stiff and the correlated flux grain size is large and involves many pinning centers. In this limit, the bulk pinning force is small, as in the infinitely stiff FLL limit described previously. As the pinning force increases relative to the inter-flux-line forces, the correlated grains become smaller and approach a limiting grain size equal to the mean pinning center spacing, so that each flux lattice grain interacts with only one pinning center. In this limit, the bulk pinning force is at its maximum, because each pinning center is applying a maximal constraint on the FLL. The bulk pinning force is close to the direct summation pinning force in this limit.

In summary, then, the central problem of summation theory is how one combines the effects of the individual fluxon-pinning center interactions and the interfluxon forces to produce a bulk pinning force to hold the FLL against the Lorentz force. Although the limiting cases of direct summation and the rigid FLL are well understood, the behavior of real materials is less clear. Several models for summation have been proposed, primarily the FLL shear and the collective-pinning models, and validation of them with experimental measurements shows that they all have some merit, but none are capable of a complete description of the origins of the bulk pinning force. A final tool for understanding the physical mechanisms behind the pinning force and J_C is scaling laws.

Scaling Laws for Flux Pinning

Experimentally it has been found that as the testing temperature is varied, many superconductors exhibit scaling of the bulk pinning force density versus applied magnetic field (28). This is observed by first measuring the J_C as a function of magnetic field and developing a curve of the bulk pinning force density versus magnetic field using Eq. (15): $F_P = J_C B$. This curve has a characteristic shape. It is zero at zero applied field, increases through a maximum with increasing field, and drops to zero again as the J_c drops to zero at $H = H_{C2}$ (Fig. 14).

As the test temperature changes, the H_{C2} of the sample changes, and as a result, the bulk pinning force changes at a given applied field. By scaling the ordinate using the reduced field, $h = H/H_{C2}$, and scaling the abscissa as the reduced pinning force density, $f_P = F_P/F_{P\,MAX}$, where $F_{P\,MAX}$ is the maximum measured bulk pinning force density, the experimental data frequently collapse onto a single line for all test temperatures (Fig. 14).

Although the majority of the experiments on scaling J_C have been performed in low temperature superconductors, a large literature has also developed for scaling behavior in high temperature superconductors. The terminology used in HTS materials has evolved along different lines than those used here, but the basic result is that temperature scaling of the pinning force is also a common feature of these materials (29,30).

It is important that the pinning force follows a scaling law with changes in magnetic field and temperature because scaling implies a single mechanism for flux pinning in the material as a function of temperature, which should be amenable to theoretical prediction. Additionally, if scaling holds for a given material, one only needs to measure the critical current at one temperature and field to estimate the performance at

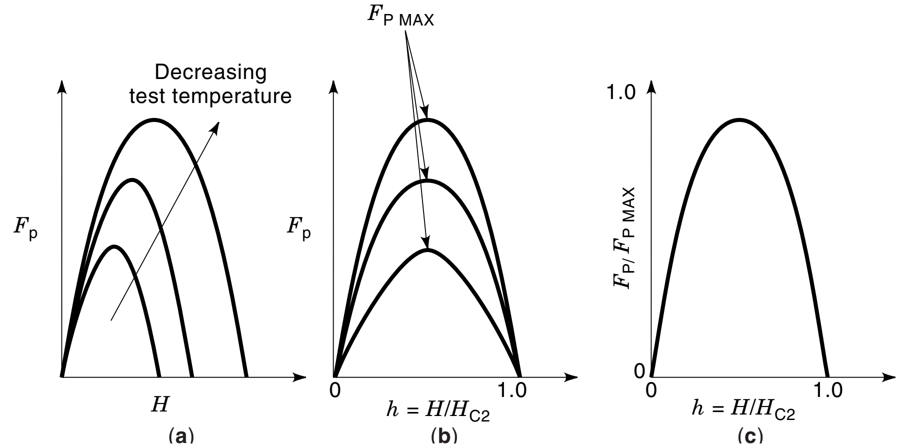

Figure 14. To determine whether a superconducting material displays scaling of the flux pinning curve, the pinning force density versus applied field for several different test temperatures is measured (a). The data are scaled using $h = H/H_{C2}$ (b) and $f_P = F_P/F_{PMAX}$ (c). If the sample displays scaling, the different temperatures collapse onto a single plot (c).

other temperatures, which can be useful for magnet designers.

In general terms, scaling follows an equation, such as

$$F_P = K(H_{C2})^m f(h) \tag{21}$$

where K and m are empirically determined constants, $f(h)$ is a function only of reduced applied field, and the temperature dependence is carried in the variation of H_{C2}. Typically in LTS materials, m varies between 1.5 and 2.5. The field function $f(h)$ may display many different kinds of scaling behavior with magnetic field (31). The two most common are the linear scaling and the quadratic scaling functions.

In linear scaling, the field function is given by

$$f(h) = h(1-h) \tag{22}$$

This is a symmetrical function of reduced field that has a peak in the pinning force density at $h = 0.5$. Often, optimized Nb-Ti superconductors follow a linear scaling behavior (32).

The quadratic scaling field function is expressed by

$$f(h) = h^{1/2}(1-h)^2 \tag{23}$$

which displays a peak pinning force density at $h = 0.25$ and a strong quadratic curvature as the applied field nears H_{C2}. The quadratic behavior is usually associated with Nb_3Sn and other single-phase superconductors (33).

Because many superconductors exhibit scaling, it is interesting to see if a theoretical model can predict the measurements and provide some insight into flux pinning behavior. Because the theoretical picture of summation is somewhat diverse, it is not surprising that the theory of pinning force density scaling is not completely clear. However, there are qualitative models that explain some of the experimental behavior.

Campbell and Evetts (7) examined the low field region of the pinning force curve, which is roughly linear with field for nearly all of the scaling models and experiments. In this region, there are a small number of flux lines compared to the number of pinning centers. Campbell and Evetts propose that direct summation should apply because the spacing between flux lines is large enough that the interactive forces between them are weak. As the field is increased from zero, the bulk pinning force density increases linearly because of the increased number of flux lines being pinned. This is often referred to as the "partial synchronization" range of fields because the flux lines become "synchronized" with the pinning center array.

At some magnetic field, the number of flux lines is equal to the number of pinning centers, and the maximum bulk pinning force density is reached. Therefore, the field of the pinning peak depends on the number of pinning centers, and the magnitude of the peak depends on the strength of the basic interactive forces (Fig. 15).

At higher fields, there are more flux lines than pinning centers, and one expects a crossover from synchronization to where the bulk pinning force is limited by other effects. In the Campbell and Evetts model the high field pinning force falls off because of the variation of the basic interactive force with field, which falls as $(1 - h)$ for the core interaction. Thus, Campbell and Evetts predict a linear low field region, a pinning peak at a field determined by the number of pinning centers, and a linear high field region. As the basic interactive force increases, the pinning force curve increases in all fields.

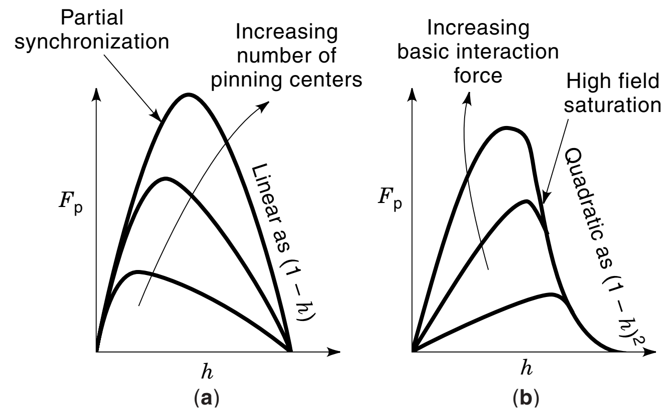

Figure 15. In the summation model of Campbell and Evetts, the pinning force curve is linear at both low fields and high fields, and the position of the peak pinning force density shifts depending on the number of pinning centers in the superconductor (a). The Kramer model, on the other hand, shows a quadratic high field behavior, and the pinning force density saturates at high fields, as the strength of the basic interaction increases (b).

An alternative model of summation due to Kramer (25) describes the low field portion of the pinning force curve by partial synchronization, as in the Campbell and Evetts model. However, the high field behavior is determined by the shear of the flux lattice past strongly pinned individual fluxons. Therefore, the high field pinning force has a magnetic field dependence determined by the C_{66} elastic constant, which from Eq. (20) decreases as $(1 - h)^2$. Kramer also predicts that the high field behavior will exhibit saturation such that variations in processing leading to changes in the basic interactive forces will affect the magnitude and position of the peak but will not affect the high field pinning force behavior (Fig. 15).

In most flux pinning theories the basic interactive force is a function of temperature. For instance, in the core pinning model, the basic interactive force depends on the condensation energy and therefore on H_C. As the temperature changes, so does H_C. This leads to the observed temperature scaling of F_P.

However, the temperature dependence is more complicated for some basic interactions. For example, if the pinning center were a superconducting precipitate with T_C and H_{C2} below that of the bulk material, one would expect a difference in the strength of the core pinning interaction as the temperature is varied above and below the pinning center critical temperature and as the field moves above and below H_{C2} of the pinner. This effect is normally observed as a lack of scaling and commonly as a shift of the peak in the pinning force curve as a function of temperature.

A second example of a lack of scaling is a superconductor in which the pinning force on the FLL is a combination of several different basic interactive mechanisms. Such a superconductor might be a two-phase alloy in which pinning results from both core interactions with normal precipitates and grain boundary pinning. The different temperature and field dependencies of the two operating pinning mechanisms lead to a lack of scaling (34).

The main points to understand from this overview of the flux pinning mechanism are the following:

- Bulk flux pinning depends on the basic interactive forces between individual flux lines and individual pinning centers.
- Bulk flux pinning depends on the relative strength of the basic interactive forces and the fluxon-fluxon forces, which affects the summation of the individual interactions into the bulk pinning force acting on the FLL.
- Scaling, or lack of scaling, provides a tool for understanding the pinning mechanisms operating in different field and temperature regions. This understanding can help direct modifications of the pinning microstructures by using suitable processing to optimize the pinning force and J_C of hard superconductors.

THE CRITICAL STATE MODEL OF MAGNETIZATION

The previous discussion has centered on the electrical behavior of the superconductor, but magnetic behavior is also an important aspect of many applications. The magnetic response of the superconductor can be a valuable tool for measuring the critical current density.

An important consequence of pinning the magnetic FLL is that the magnetic behavior of hard superconductors is strongly hysteretic (Fig. 16). To understand the development of the hysteretic magnetization curve, a simple but powerful model was proposed by Bean (35) and has since been modified and further refined (36).

To simplify discussion of the model, we use a sample geometry of an infinite superconducting plate of thickness W. The applied magnetic field will be parallel to the surfaces of the plate, as in Fig. 17. As the magnetic field is increased from zero, superconducting magnetization currents develop on the surfaces, so that they shield the interior of the superconductor from the applied field (the Meissner–Ochsenfeld effect). These shielding currents flow only within a distance λ (the penetration depth) of the surface and fall off exponentially into the superconductor. This condition persists until the external applied field exceeds the lower critical magnetic field H_{C1}. For fields larger than H_{C1} the superconductor is thermodynamically more stable if the applied field enters the superconductor as the flux line lattice. For simplification, the Meissner state below H_{C1} is ignored in the critical state model. This is not a bad approximation, especially for the technological superconductors which have large values of the Ginzburg–Landau parameter κ and therefore small values of H_{C1}.

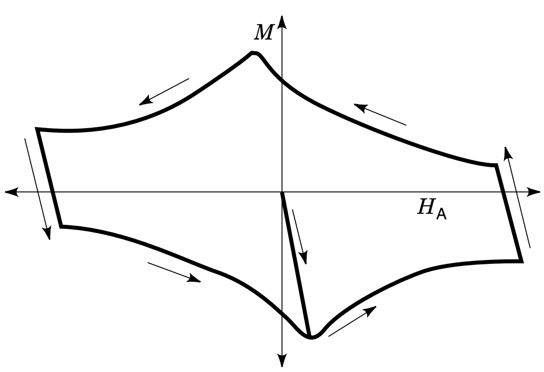

Figure 16. Schematic of the hysteretic magnetization curve in strong pinning superconductors. The arrows indicate the direction of travel around the hysteresis loop during a typical magnetization measurement.

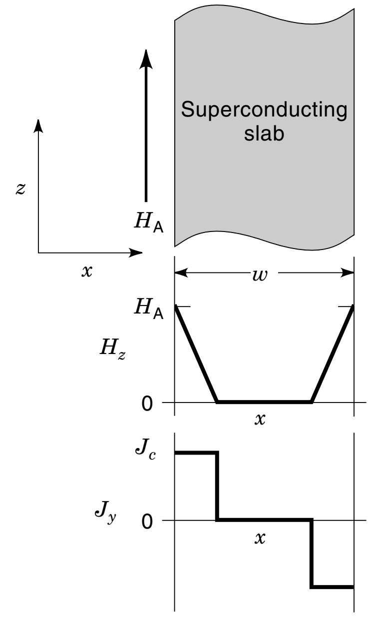

Figure 17. In the Bean critical state model, the semi-infinite slab develops the flux and current density profiles shown on the application of a magnetic field larger than H_{C1}.

If the sample has pinning centers to hold the entering FLL in place, a magnetic field gradient is established at the surface of the superconductor which falls off into the body of the sample. From earlier discussions of Ampere's law, we know that the current density flowing in a superconductor is directly related to the magnetic field gradient, Eqs. (9) and (10). The situation looks schematically like that shown in Fig. 17, where the z-directed applied field falls off into the sample with a gradient in the x-direction that produces a current density flowing in the y-direction (into the page).

The current density flowing is equal to the critical current density. If the flux gradient were steeper, the current density would be larger than the J_C, and the FLL would not be fully pinned, leading to flux flow. The flux motion lowers the field gradient until the FLL is pinned by the pinning centers, leaving a critical flux gradient and a current density equal to J_C. For this reason the model is known as the "critical state model."

In Bean's original version of the critical state model, the J_C is assumed to be a constant, independent of applied field from $H_{C1} < H_A < H_{C2}$. This assumption makes the flux profile in the sample linear such that

$$\frac{dH_z}{dx} = \frac{\Delta H_z}{\Delta x} = J_y = \text{constant} = J_C \tag{24}$$

As the applied field is increased from $H_A = 0$, the field penetrates the sample from both sides, and generates a circulating shielding current equal to J_C (Fig. 17). The magnetization of the slab can be found from examination of the field versus position plot. From the definition of magnetization, we know that the local magnetization response of the superconductor to the applied field can be written as the difference between the applied field and the local internal magnetic field:

$$M(x) = H_I(x) - H_A \tag{25}$$

where $H_I(x)$ is the local internal magnetic field. To find the bulk magnetization, we must integrate the local magnetization over the sample volume. Because the sample is infinite in the y- and z-directions, we can turn this into a one-dimensional integral over x, such that

$$\begin{aligned} M_{\text{bulk}} &= \left(\frac{1}{W}\right)\int H_I(x)\,dx - \left(\frac{1}{W}\right)\int H_A\,dx \\ &= \left(\frac{1}{W}\right)\int [H_I(x) - H_A]\,dx \end{aligned} \tag{26}$$

Comparing Eq. (26) with Fig. 18 shows graphically that the second term is the area of the entire rectangular region, whereas the first term is given by the area of the two darker triangular regions. The bulk magnetization is the volume averaged difference between these, or the light gray trapezoidal area of Fig. 18, divided by the sample width W.

Using this simple model we can determine the behavior of the superconductor during a half magnetic field cycle used to generate a magnetization loop of M versus H_A. The process is shown schematically in Fig. 19. For small applied fields (points a, b) the field penetrates, and the magnetization increases rapidly with applied field. At point c the applied field is large enough to push the magnetic flux line lattice all the way to the center of the sample. This field is called the full penetration field H_P.

For applied fields larger than the full penetration field, the magnetization does not change, even though the internal and external fields increase. The magnetization curve remains flat (points d, e).

Now, if the applied field were to be reduced, the flux lattice, which is being pinned in place by the pinning centers, responds only near the surface region, as shown at point f. The magnetization becomes rapidly smaller with decreasing field. Now, the circulating supercurrents flowing in the sample have the spatial dependence shown in Fig. 20. Both the positive and negative flowing currents are assumed to be flowing at the critical current density. Recall that the magnitude of the critical current density in the Bean critical state model is constant with magnetic field.

As the applied field is further reduced, the current density profile eventually inverts, and the magnetization becomes positive and constant (g). Finally, at $H_A = 0$, the magnetization is positive because of the magnetic fields trapped in the body of the superconductor by the pinning forces acting on the FLL.

Because the flux gradient is a constant, the full penetration field H_P, varies with the width of the sample. Examina-

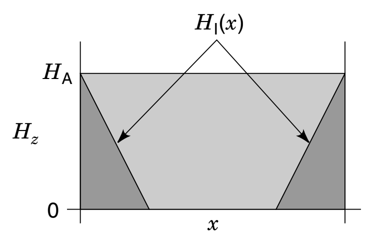

Figure 18. The flux profile in the superconductor on applying a field H_A. This is useful for understanding the origin of the terms in the integral of Eq. (26). The magnetization response to the applied field H_A is proportional to the area of the light gray trapezoid.

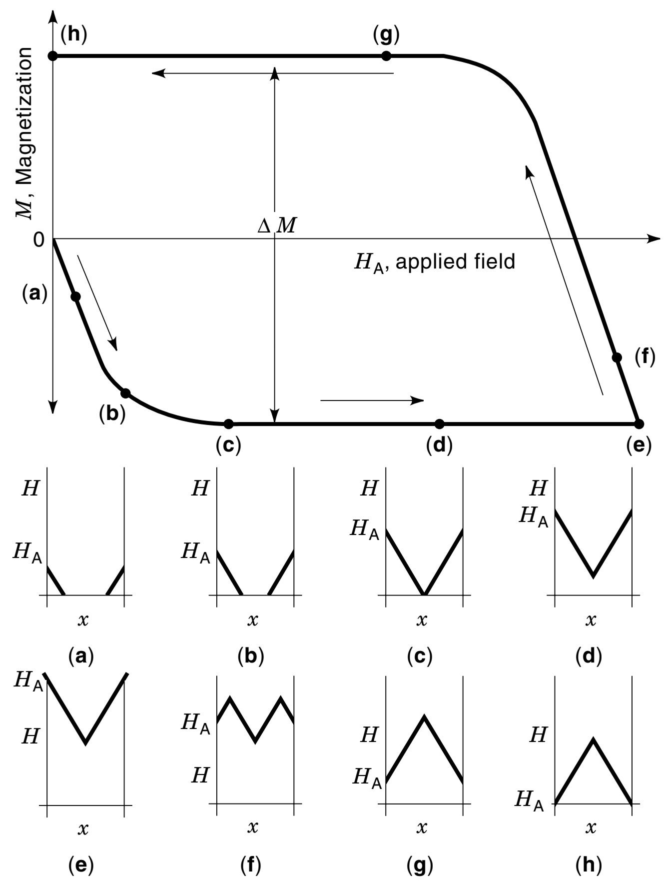

Figure 19. Schematic of a half hysteresis loop measurement of the magnetization in a Type II superconductor. The flux profiles at eight points around the magnetization loop are derived from the Bean critical state model and illustrate the source of the dependence of the magnetization on the pinning of magnetic flux within the superconductor.

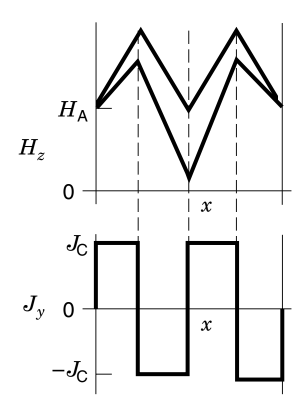

Figure 20. The flux profile and the accompanying current density profile for point (f) of Fig. 19. The current density profile matches the profile of the magnetic flux at all points in the superconductor.

tion of Fig. 19 at the full penetration field (point c) shows that the magnetic flux gradient

$$\frac{dH}{dx} = -\frac{H_P}{(W/2)} = J_C \tag{27}$$

We can also see that the magnitude of the magnetization at this field is given by

$$M(H_P) = \frac{2}{W}\int\left[\left(H_P + x\frac{dH}{dx}\right) - H_P\right]dx = \frac{J_C}{\left(\frac{W}{2}\right)}\int x\,dx \tag{28}$$

integrated from $x = 0$ to $W/2$. This gives the constant value of the magnetization with applied field (points c, d, e) as

$$M = J_C\left(\frac{W}{2}\right) \tag{29}$$

Figure 19 also illustrates that, when one considers the entire hysteresis loop of the magnetization measurement, the distance between the increasing field and decreasing field magnetization at any applied field is twice the result of Eq. (29), or the more usual result from the critical state model,

$$\Delta M = J_C W \tag{30}$$

The Bean critical state model has been modified to account for the fact that the critical current density is not a constant with applied field (36). These modifications lead to curved magnetic field and current density profiles (Fig. 21) in addition to more realistic magnetization loops (Fig. 16). It is still

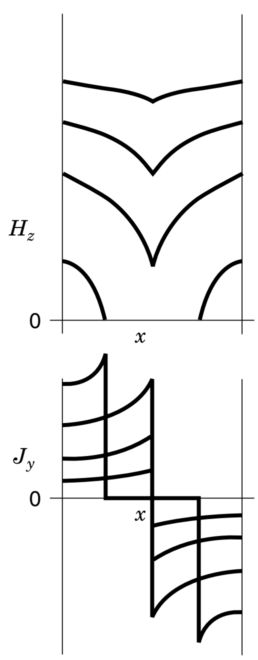

Figure 21. The Bean critical state model assumes that the critical current density is constant with the magnetic field. In modified versions of the critical state model, the critical current density is allowed to vary with the magnetic field. The effects on the magnetic flux profiles and accompanying current density profiles are shown here for four different applied fields. As the applied field becomes larger, the critical current decreases. The slope of the flux profile changes with the magnetic field, and it is also no longer linear with position in the superconductor.

the case, however, that these models predict a direct relationship between the height of the magnetization loop at a given field and the critical current density multiplied by the sample dimension.

Other modifications to the Bean Critical State Model have incorporated the change in magnetization due to finite sample sizes (37) and demagnetization factors for non-spherical samples (38).

The most important result of the Bean model is that the magnetization behavior can be used as a probe of the critical current density within the superconductor by using a technique different from the four-point resistive measurement. For many emerging superconducting materials, magnetization measurements have allowed measuring the critical current density before long lengths of wire were available for resistive testing. It is also possible to measure J_Cs that would be difficult to measure with a conventional resistive technique. An example is a cabled conductor with an I_C of thousands of amperes. Multikiloamp power supplies are expensive to purchase and operate, and the high current significantly complicates the experimental design. Magnetization measurements of J_C are not limited by the need for high current power supplies. The magnetization measurement of J_C continues to be an important tool for the materials engineer in optimizing the flux pinning process.

DISSIPATION EFFECTS IN HIGH CURRENT DENSITY SUPERCONDUCTORS

The movement of the FLL within the superconductor has many consequences for the applications of superconductors. Examples include flux jumping (the rapid movement of magnetic flux within the superconductor which leads to localized heating effects and the loss of the superconducting state), flux flow near the J_C, flux creep (the slow movement of the FLL caused by random thermal jumping of flux lines out of the pinning potentials), and magnetic hysteresis (which causes an additional heating effect and resistive loss in ac applications of superconductors). Because of their importance to applications, the dissipative effects have been carefully studied and have led to some useful insights into the flux pinning process.

Flux Flow and Resistive Transition Analysis

As we have seen previously, the transition from the flux pinning to the flux flow state is generally not sharp but occurs over a range of currents during a resistive critical current measurement. Several models for the shape of the resistive transition have been developed to account for this behavior (39–41), but they all assume a distribution of pinning center strengths within the wire. The idea was first proposed by Baixeras and Fournet (42) but was not fully developed and applied to technological superconductors until the 1980s. If one assumes that the superconducting wire is made of an assortment of independent, current-carrying segments in series, each with its own value of critical current (as determined by the flux pinning defects within each segment), then the equation for the $V(I)$ curve can be written as

$$V(I) = A\int(I - I')f(I')\,dI' \tag{31}$$

where I' is the local critical current of an individual wire segment, A is a constant, $f(I)$ is the critical current distribution of the segments in the wire, and the integral is performed from zero current to I.

In essence this states that the voltage at any transport current I results from the segments with $I_C < I$ and are therefore in flux flow. Variations in the critical current of each segment may occur because of variations in processing, chemical inhomogeneities, or changes in geometry. For wires that are very homogeneous along their lengths, the distribution in critical currents $f(I)$ is very narrow, and the $V(I)$ characteristic is quite sharp and steep, leading to large n-values and the associated measure of "high-quality" in technological superconductors (43). At the other extreme, a large variation in the critical current distribution leads to a broad $V(I)$ transition and a low n-value.

The importance of the model for helping the development of high J_C superconductors is that it can be used in reverse to determine the critical current distribution function from a measurement of the $V(I)$ curve. By taking the second derivative of both sides of Eq. (31),

$$\frac{d^2V}{dI^2} = Af(I) \tag{32}$$

The second derivative of the experimentally determined $V(I)$ curve yields the distribution $f(I)$ of critical currents within the sample. In practice it is found that the resistive critical current measurement is always at a current well below the peak of the critical current distribution $f(I)$. Technological superconductors are limited by the weakest flux pinning segment along the sample length.

Temperature Dependence: Flux Creep and FLL Melting

As the temperature of a strongly pinned superconductor is increased, the thermal energy available to the pinned flux lines increases, allowing the possibility of thermally induced flux depinning. The higher temperatures lead to thermal excitation of the flux lines within the pinning potential wells. In low temperature superconductors where the thermal energies are low, the thermal energy is typically much smaller than the depth of the pinning potential. This led early investigators to name the effect "flux creep" because of the similarity to mechanical creep of crystalline materials at stresses much lower than the yield stress.

The theory and model for flux creep was developed by Anderson (44) and elaborated by Kim and Anderson (45). The basic premise is that flux lines at any finite temperature, experience a thermal excitation due to the thermal energy kT. The excitation energy has a statistical probability of causing a flux line pinned by a pinning center to become unpinned. The probability of this thermal depinning occurring is given by the Arrhenius factor

$$p = \exp\left(-\frac{U}{kT}\right) \tag{33}$$

where U is the depth of the energy well of the pinning center (Fig. 10).

For an isolated flux line, assuming no temperature gradient, there is no preferred jump direction because both the pinning potential and the thermal excitation are spatially symmetrical. Thus the flux line would execute a random walk as the thermal excitation allowed it to leave the pinning potentials, and no net change in flux would occur.

For a flux line in a magnetic field gradient, the flux motion associated with the thermal activation of the flux line derived from a diffusion argument is

$$\frac{dB}{dt} = Aw_0 \exp\left(-\frac{U}{kT}\right) \tag{34}$$

where A is a factor that depends on the local magnetic field and field gradient and w_0 is the frequency with which the flux line tries to jump out of the well.

The flux gradient provides a driving force that leads to diffusion of the flux line preferentially down the flux gradient. This produces a changing magnetic flux density according to Eq. (34) which can be experimentally measured. The flux gradient can exist because of the presence of either a transport current or a magnetization current in the sample.

In the case of a magnetization-induced flux gradient, the flux gradient would decay, eventually disappearing, even though the flux gradient (or magnetization current density) is less than the critical current density. This is in contrast to the assumptions of the Bean critical state model, in which the flux gradient adjusts itself to match the critical current density at all points in the sample. In the original experimental work on flux creep (46), the measured decay of the magnetization currents translated into a decay time of 10^{92} years, effectively infinite time, so that, even with flux creep, the persistent magnetization supercurrents that flow as a result of the Meissner–Ochsenfeld effect are truly persistent.

The situation is somewhat different when the flux gradient driving force is produced by an externally applied transport current. In this case, the flux gradient crosses the superconductor, and the effect of the flux creep is to move flux lines across the sample in a manner identical to the flux depinning process at J_C. In the same way that the FLL motion causes a resistive-like dissipation in the superconductor, the flux creep motion also contributes to the dissipation. This results in a power loss in the superconductor that must be supplied by the external power supply and a consequent heating of the superconductor caused by the flux motion. If the flux motion is too great, the temperature increases, which increases the probability of thermally activated flux motion, and a thermal runaway to the normal state ensues.

At higher temperatures, the thermal excitation of the flux lines becomes comparable to the pinning potential, and the FLL is expected to move more easily. This, in fact, was one early argument against the possibility of technologically important superconductors at high temperatures. The argument was that no known basic pinning interactions are strong enough to prevent thermal excitation of the FLL at high temperatures (e.g., at 77 K, liquid nitrogen), even at very small transport currents. Fortunately for high temperature superconductors, this has not been the case. However, the concerns about the higher thermal energy available for excitation of the FLL out of the HTS pinning centers led along a path different from the original flux creep models into the theories of flux lattice melting.

Much of the theoretical picture of thermal effects on the FLL in HTS materials is at heart the same as in low temperature materials. The basic interests are in the possibility of scaling the pinning force with temperature, magnetic field dependence of the J_C, and the importance of the higher thermal energy in the depinning and motion of the FLL. The terminology has developed differently, but the physical mechanisms of flux pinning and depinning do not differ substantially.

SUMMARY AND CONCLUSIONS

The critical current density of superconducting materials is a technologically important parameter, often more important in engineering design than the T_C or the H_{C2}. The theory of the J_C is broad and has provided useful insights into the physical mechanisms responsible for the large values of critical current density found in technological superconductors. This article has described the standard resistive and magnetic measurements of critical current. The theories of superconducting critical current range from the ultimate limits to the J_C, as described by the depairing current density, to the limits imposed by the thermal excitation of flux lines out of their pinning centers. The development of a bulk pinning force from the summation of individual pinning center interactions leads to the empirically observed scaling laws for the J_C that are important both as a tool for understanding the flux pinning processes and as an extrapolating technique useful for technological design.

Ultimately, this article has attempted to show the connection between the measured values of the J_C and the microstructural defects responsible for pinning the magnetic flux-line lattice in place. Understanding the physical processes underlying the development of the J_C has led materials engineers to design fabrication and processing that produces the desired microstructural features necessary for high J_C. In the past 10 to 15 years, this has led to massive increases in the performance of superconducting materials for applications requiring high current density and promises additional improvements in the future.

BIBLIOGRAPHY

1. M. N. Wilson, *Superconducting Magnets,* Oxford, UK: Oxford University Press, 1983.
2. D. C. Larbalestier, in S. Foner and B. B. Schwartz (eds.), *Superconductor Materials Science: Metallurgy, Fabrication and Applications,* New York: Plenum Press, pp. 133–200, 1981.
3. M. Suenaga, in S. Foner and B. B. Schwartz (eds.), *Superconductor Materials Science: Metallurgy, Fabrication and Applications,* New York: Plenum Press, pp. 201–274, 1981.
4. A. C. Rose-Innes and F. H. Rhoderick, *Introduction to Superconductivity,* Oxford, UK: Pergamon, 1969.
5. M. Tinkham, *Introduction to Superconductivity,* New York: McGraw-Hill, 1975.
6. T. P. Orlando and K. A. Delin, *Foundations of Applied Superconductivity,* Reading, MA: Addison-Wesley, 1991.
7. A. M. Campbell and J. E. Evetts, *Adv. Phys.,* **21**: 199–428, 1972.
8. H. Ullmaier, *Irreversible Properties of Type II Superconductors,* Berlin: Springer-Verlag, 1975.
9. Y. B. Kim, C. F. Hempstead, and A. R. Strnad, *Phys. Rev.,* **139** (4A): 1163–1172, 1965.
10. F. Volker, *Particle Accelerators,* **1**: 205–207, 1970.
11. H. K. Olsson et al., *Phys. Rev. Lett.,* **66** (20): 2661–2664, 1991.
12. N.-C. Yeh et al., *Phys. Rev. B,* **45** (10): 5710–5713, 1992.
13. T. S. Kreilick, Niobium-Titanium Superconductors, in *Metals Handbook,* Vol. 2, 10th edition, Materials Park, OH: ASM International, pp. 1043–1059, 1990.
14. F. B. Silsbee, *J. Wash. Acad. Sci.,* **6**: 597, 1916.
15. A. A. Abrikosov, *Sov. Phys. JETP,* **5**: 1174, 1957.
16. U. Essman and H. Trauble, *Phys. Lett.,* **24A**: 526–527, 1967.
17. J. D. Cribier et al., *Progress in Low Temperature Physics,* Vol. V, C. J. Gorter (ed.), Amsterdam: North-Holland, 1967, p. 161.
18. G. Zerweck, *J. Low Temp. Phys.,* **42** (1): 1–9, 1981.
19. A. Gurevitch and L. D. Cooley, *Phys. Rev. B,* **50** (18): 13563–13576, 1994.
20. L. D. Cooley, P. J. Lee, and D. C. Larbalestier, *Phys. Rev. B,* **53** (10): 6638–6652, 1996.
21. H. Trauble and U. Essmann, *Phys. Stat. Sol.,* **25**: 395–402, 1968.
22. J. Schelten, H. Ullmaier, and G. Lippmann, *Phys. Rev. B,* **12** (5): 1772–1777, 1975.
23. E. H. Brandt, *J. Low Temp. Phys.,* **21**: 709, 1977.
24. E. J. Kramer, *J. Appl. Phys.,* **44** (3): 1360–1370, 1973.
25. E. J. Kramer, *J. Electron. Mater.,* **4** (5): 839–881, 1975.
26. A. I. Larkin and Yu. N. Ovchinikov, *J. Low Temp. Phys.,* **34**: 409–428, 1979.
27. R. Labusch, *Cryst. Lattice Defects,* **1**: 1–16, 1969.
28. W. A. Feitz and W. W. Webb, *Phys. Rev.,* **178** (2): 657–667, 1969.
29. M. P. A. Fisher, *Phys. Rev. Lett.,* **62** (12): 1415–1418, 1989.
30. B. Brown et al., *Phys. Rev. B,* **55** (14): 8713–8716, 1997.
31. D. Dew-Hughes, *Philos. Mag.,* **30**: 293–305, 1974.
32. D. G. Hawksworth and D. C. Larbalestier, *Proc. 8th Symp. Eng. Probl. Fusion Res.,* 1979, Vol. 1, p. 245.
33. R. J. Hampshire and M. T. Taylor, *J. Phys. F,* **2**: 89–106, 1972.
34. C. Meingast, P. J. Lee, and D. C. Larbalestier, *J. Appl. Phys.,* **66** (12): 5962–5970, 1989.
35. C. P. Bean, *Phys. Rev. Lett.,* **8**: 250–253, 1962.
36. D.-X. Chen and R. B. Goldfarb, *J. Appl. Phys.,* **66** (6): 2489–2500, 1989.
37. R. B. Goldfarb and J. V. Minervini, *Rev. Sci. Instrum.,* **55** (5): 761–764, 1984.
38. M. Daumling and D. C. Larbalestier, *Phys. Rev. B,* **40** (13): 9350–9353, 1989.
39. J. E. Evetts and C. J. G. Plummer, *Proc. Intl. Symp. Flux Pinning Electromagnetic Properties Superconductors,* T. Matsushita, (ed.), Fukuoka, Japan: Matsukama Press, 1986, p. 150.
40. D. P. Hampshire and H. Jones, *Proc. 9th Intl. Conf. Magnet Technology,* C. Marinucci (ed.), Swiss Institute for Nuclear Research, Geneva, Switzerland, 1985, p. 531.
41. W. H. Warnes and D. C. Larbalestier, *Appl. Phys. Letts.,* **48** (20): 1403–1405, 1986.
42. J. Baixeras and G. Fournet, *J. Phys. Chem. Solids,* **28**: 1541, 1967.
43. W. H. Warnes and D. C. Larbalestier, *Cryogenics,* **26** (12): 643–653, 1986.
44. P. W. Anderson, *Phys. Rev. Letts.,* **9** (7): 309–311, 1962.
45. P. W. Anderson and Y. B. Kim, *Rev. Mod. Phys.,* **36**: 39, 1964.
46. Y. B. Kim, C. F. Hempstead, and A. R. Strnad, *Phys. Rev. Lett.,* **9** (7): 306–311, 1962.

WILLIAM H. WARNES
Oregon State University